Available online at www.sciencedirect.com

ScienceDirect

Advances in Space Research xxx (2017) xxx–xxx

ELSEVIER

ADVANCES IN SPACE RESEARCH (a COSPAR publication)

www.elsevier.com/locate/asr

A quantitative method to evaluate the performance of topographic correction models used to improve land cover identification

Sung-Hwan Park [a], Hyung-Sup Jung [a], Jaewon Choi [b], Seongwoo Jeon [c,*]

[a] *Department of Geoinformatics, University of Seoul, South Korea*
[b] *Pine Wilt Disease Monitoring Center, Korea Forestry Promotion Institute, South Korea*
[c] *Division of Environmental Science & Ecological Engineering, Korea University, South Korea*

Received 7 February 2017; received in revised form 24 June 2017; accepted 29 June 2017

Abstract

Topographic correction methods have been widely used prior to land cover identification in sloping terrain because the topographic variation on the Earth's surface can interfere with the classifications. The topographic correction involves the normalization of brightness or surface reflectance values from the slanted to the horizontal plane. Several topographic correction models have been proposed, and a quantitative evaluation method is needed for these models because the performance can vary according to the surface cover types and spectral bands. In this study, we proposed an efficient method to evaluate the performance of topographic correction models through measuring the histogram structural similarity (HSSIM) index estimated from the sunlit and sun-shaded slope areas before and after the correction. We tested the HSSIM index by using three different land cover types derived from Landsat-8 Operational Land Imager (OLI) images and eight commonly used topographic correction models. When the proposed HSSIM index was compared with the visual analysis technique, the results matched exactly. Using the HSSIM index, the best correction methods were then determined, and the best ones included the statistical-empirical or SCS+C methods (where SCS+C refers to the sun-canopy-sensor plus C-correction) for the R, G, and B bands and the Minnaert+SCS method for the NIR, SWIR-1, and SWIR-2 bands. These results indicate that (i) the HSSIM index enables quantitative performance evaluations of topographic correction models and (ii) the HSSIM index can be used to determine the best topographic correction method for particular land cover identification applications.

Keywords: Topographic correction models; Land cover identification; Performance assessment

1. Introduction

Remotely sensed images have been widely used for land cover identification (Srivastava et al., 2012; Moreira and Valeriano, 2014; Wei et al., 2017). Many identification methods have been proposed, and over time, these methods have achieved remarkable performance improvements (Szuster et al., 2011; Srivastava et al., 2012). However, the images are affected by the topographic effect due to the location of the Sun, sensor angle, and curvature of the terrain. This effect is more intense over mountainous areas. In a mountainous area, the terrain will reflect weaker or stronger solar radiation according to the slope than the horizontal surface. Consequently, sun-shaded areas and sunlit areas can be grouped into different classes even if the land surface types of both areas are the same. This is a main factor that has hindered further improvements in land cover identification (Ren et al., 2009). Since the topo-

* Corresponding author.
E-mail address: eepps_korea@korea.ac.kr (S. Jeon).

http://dx.doi.org/10.1016/j.asr.2017.06.054
0273-1177/

graphic effect causes errors in land cover identification over mountainous areas, it needs to be corrected.

Topographic correction involves the normalization of brightness or surface reflectance values from the slanted to the horizontal plane (Richter, 1997, 1998). The topographic correction methods that have been developed can be categorized according to surface reflection types (Ediriweera et al., 2013; Singh and Talwar, 2013). The first category assumes that the ground surface is a Lambertian surface that reflects solar energy equally in all directions. However, because this approach is very unrealistic, it often leads to underestimations or overestimations (Mishra et al., 2009). In the Lambertian approach, cosine correction (Teillet et al., 1982), sun-canopy-sensor (SCS) correction (Gu and Gillespie, 1998), and C-HuangWei correction (Huang et al., 2005) techniques can be applied. The second category involves non-Lambertian (semi-empirical) methods, in which surfaces are modeled by using additional parameters. The non-Lambertian approach can be used in conjunction with the C-correction (Teillet et al., 1982), SCS+C correction (Soenen et al., 2005), and Minnaert and Minnaert+SCS correction techniques (Smith et al., 1980; Reeder, 2002). The final category involves empirical methods, which use an empirically determined calibration coefficient. The statistical-empirical model is a commonly used empirical method (Teillet et al., 1982). Further comparisons and details of the topographic correction methods can be found in the literature (Smith et al., 1980; Teillet et al., 1982; Meyer et al., 1993; Gu and Gillespie, 1998; Reeder, 2002; Huang et al., 2005; Soenen et al., 2005; Gao and Zhang, 2009; Mishra et al., 2009; Reese and Olsson, 2011; Gao et al., 2014).

The performance of the topographic correction models is largely dependent on land surface types (Goslee, 2012; Singh et al., 2015). Thus, the best topographic correction model may change according to the land surface types of a study area. Consequently, it is quite necessary to choose the best model for a given image. The best model selection process plays an important role in achieving high object-based identification accuracies (Vanonckelen et al., 2013; Moreira and Valeriano, 2014). Performance evaluations of topographic correction models have been be carried out by (i) using in-situ measurements, (ii) comparing the land cover identification before and after topographic corrections, and (iii) applying simple statistical analyses (Mishra et al., 2009; Moreira and Valeriano, 2014). The evaluations based on in-situ measurements are associated with high costs and time-consuming procedures (Reese and Olsson, 2011; Zhang et al., 2011). The before and after identification approach has been widely used to assess the correction performance (Dorren et al., 2003; Blesius and Weirich, 2005; Gao and Zhang, 2009; Reddy and Blah, 2009; Vanonckelen et al., 2013), but it does not allow us to evaluate the correction performance of each band and the results largely depend on the land cover types, numbers of bands used for identification, methods used for the bands, etc. The statistical approaches have been carried out by using simple statistical parameters such as the mean, standard deviation (SD), coefficient of determination (r^2), root mean square error (RMSE), etc. (Gu et al., 1999; Tokola et al., 2001; Dorren et al., 2003; Riano et al., 2003; Vincini and Frazzi, 2003; Moreira and Valeriano, 2014). However, simple statistical parameters are not rigorous enough for evaluations of the performance of topographic correction models. One of the most widely used evaluation methods involves the quantification of the reduction of the dependence between $\cos i$, the incidence angle, with respect to the normal surface. In this method, researchers measure the slope of the linear regression between $\cos i$ and values of a study area. If the slope of the regression is close to zero, the data are assumed to have been successfully corrected (Gao and Zhang, 2009). However, this method is not valid for land surfaces where slope orientation determines the land cover or growth stage (Hanston and Chuvieco, 2011). Recently, an evaluation method called the structural similarity (SSIM) index has been proposed by Sola et al. (2014). This method compares the luminance, contrast, and structural similarity between a synthetic horizontal image, which is generated by considering the ground reflected, direct, diffuse, and global horizontal irradiances, and a topographically corrected real image. However, the procedure for producing the synthetic horizontal image is complicated, yet it is required to evaluate whether the data are generated well.

The principle of topographic correction is to increase the reflectance/radiance values of the sun-shaded slopes and decrease the values of the sunlit slopes so that the values of both slopes are made similar. Thus, the topographic correction models should quantitatively evaluate how similar the values of both slopes are. In addition, the variation in dispersion after correction within the same slope should also be assessed, and it should be shown how much the image has been corrected based on the original image. In other words, it is necessary to evaluate the topographic correction models from the above three viewpoints.

In this study, we propose a quantitative method to evaluate the performance of topographic correction models used to improve land cover identification. We introduce the histogram structural similarity (HSSIM) index, which is calculated from the difference of the standard deviations and the histograms between the sunlit and sun-shaded slope areas before and after topographic correction. Our proposed method exploits the structural similarity between the histograms of the sunlit and sun-shaded slope areas. It should be noted that the proposed HSSIM index represents the probability of identifying the same land cover areas as the same objects.

2. Study area and datasets

Three Landsat-8 Operational Land Imager (OLI) images were used for this study. Six spectral bands ranging from blue to short wavelength infrared-2 (SWIR-2) were selected for the performance evaluation of topographic corrections. The radiometric quantization of OLI (12-bit) is higher than those of the Landsat Thematic Mapper (TM) and Enhanced Thematic Mapper Plus (ETM+) (8-bit). This higher radiometric quantization allows for significant improvements, i.e., better characterizations, in the sun-shaded area (Irons et al., 2012). The surface reflectance was used instead of digital values in this study to reduce atmospheric effects in mountainous regions (Soenen et al., 2008). It was estimated by the cosine approximation (COST) atmospheric correction method (Chavez, 1996).

Test image 1 was obtained on May 26, 2015, with sun zenith and azimuth angles of approximately 23.9° and 127.8°, test image 2 was obtained on April 24, 2015, with sun zenith and azimuth angles of approximately 30.7° and 138.3°, and test image 3 was obtained on December 17, 2014, with sun zenith and azimuth angles of approximately 63.4° and 159.9°, respectively. All of the test samples for images were obtained from the north-eastern part of the Gangwon Province, South Korea, between 37°27′ and 37°53′N and 128°05′ and 128°38′E. Table 1 summarizes the characteristics of the test images, and Fig. 1 shows the three test samples. The dominant land cover types of the test samples were composed of deciduous forest, broad-leaved deciduous forest, and snow. The test samples were chosen in such a way as to allow for the consideration of common land cover types in mountainous areas.

The dominant land cover type of test sample 1 was dense deciduous forest, as shown in Fig. 1a, and the overall color was green because test image 1 was acquired during the summer season. Test sample 2 consisted of broad-leaved deciduous forest (Fig. 1b), the overall color was brown because test image 2 was acquired during the spring season. The western part of test sample 2 displayed some green color because this part consisted of coniferous forest. The dominant land cover type of test sample 3 was snow. Snow had been falling steadily in this region one month prior to the acquisition of the image. Snowfall was recorded at 5 ± 7 cm according to the Korea Meteorological Administration. This sample had a high contrast between sunlit and sun-shaded slopes because the sun zenith angle was higher than that of the other test samples as presented in Fig. 1c. Fig. 1d shows the land cover map in the test area. The land cover map was constructed from aerial photos with a spatial resolution of 5 m.

For the topographic analysis, the Shuttle Radar Topography Mission (SRTM) digital elevation model (DEM) was used (Reuter et al., 2007). The SRTM DEM provides high-quality DEM data with a ground resolution of about 30 m. The horizontal and vertical accuracies of the SRTM DEM were about 20 m and 16 m, respectively. The horizontal and vertical datum were referenced to the WGS84 (World Geodetic System 1984) and EGM96 (Earth Gravitational Model 1996) geoids, respectively (Slater et al., 2006; Su and Guo, 2014). The slope and aspect were calculated from the SRTM DEM by using the third-order finite difference weighted by the reciprocal of the squared distance algorithm (Zhou and Liu, 2004). The mean altitude was about 727 m, and it ranged from about 166 m to 1570 m in the sample area. The mean and maximum slopes were approximately 20.8° and 65.5°, respectively.

3. Methods

3.1. Short overview of the topographic correction models

Eight types of topographic correction methods were used for this study as listed in Table 2. These methods included the cosine, statistical-empirical, C-correction, SCS, SCS+C, C-HuangWei, Minnaert, and Minnaert+SCS techniques (Smith et al., 1980; Teillet et al., 1982; Gu and Gillespie, 1998; Reeder, 2002; Huang et al., 2005; Soenen et al., 2005). Both the C-correction and SCS+C models require parameter C. The role of empirical parameter C is to increase the denominator of the model equation and weaken the over-correction by adding it to the cosine correction method. Normally, C can be estimated from a linear regression analysis between the surface reflectance and the cosine of the incidence angle ($\cos i$) (Meyer et al., 1993; Gu and Gillespie, 1998). Details about the calculation of the incidence angle can be found in Robinson (1966). The relationship between the surface reflectance and incidence angle is given by:

$$\rho = m \cdot \cos i + b, \tag{1}$$

where ρ is the surface reflectance before topographic correction and m and b are the model parameters in the linear regression analysis. Then, parameter C is calculated by dividing the offset by the slope ($C = b/m$) (Teillet et al., 1982).

It is well known that the Minnaert and Minnaert+SCS models are able to effectively correct the topographic effects in mountainous regions by using the constant k (called the Minnaert constant) and k' (Reeder, 2002). The Minnaert constant k indicates the sensitivity of topographic effects according to land cover types (Gu and Gillespie, 1998). k can be calculated by linearizing the model equation as follows:

Table 1
Characteristics of the test samples of images used in this study.

Sample No.	Date	Zenith angle	Azimuth angle	Dominant land cover type
1	2015/05/26	23.90°	127.82°	Deciduous forest
2	2015/04/24	30.73°	138.33°	Broad-leaved deciduous forest
3	2014/12/17	63.36°	159.92°	Snow cover

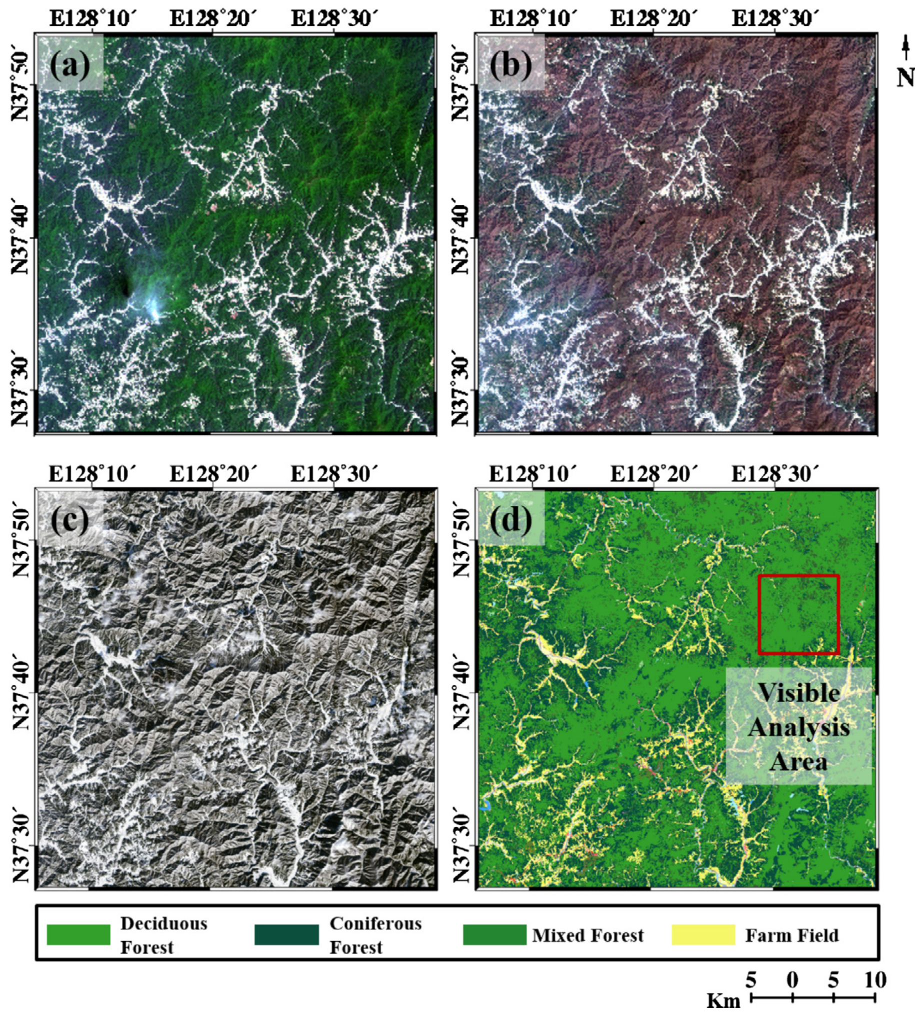

Fig. 1. Test samples in (a) deciduous forest, (b) broad-leaved deciduous forest, and (c) snow-covered areas, and (d) land cover map used for the reference data. All test samples show Landsat OLI bands 4, 3, and 2 as red, green, and blue, respectively. (For interpretation of the references to color in this figure legend, the reader is referred to the web version of this article.)

Table 2
Topographic correction models used for this study.

Topographic correction models	Model equations	References
Cosine	$\rho_h = \rho \frac{\cos\theta_s}{\cos i}$	Teillet et al. (1982)
Statistical-empirical	$\rho_h = \rho - m \cdot \cos i + m \cdot \cos\theta_s$	Teillet et al. (1982)
C-correction	$\rho_h = \rho \frac{\cos\theta_s + C}{\cos i + C}$	Teillet et al. (1982)
SCS	$\rho_h = \rho \frac{\cos\theta_s \cdot \cos\theta_n}{\cos i}$	Gu and Gillespie (1998)
SCS+C	$\rho_h = \rho \frac{\cos\theta_s \cdot \cos\theta_n + C}{\cos i + C}$	Soenen et al. (2005)
C-HuangWei	$\rho_h = (\rho - \rho_{\min})\left(\frac{\cos\theta_s - \cos i_{\min}}{\cos i - \cos i_{\min}}\right) + \rho_{\min}$	Huang et al. (2005)
Minnaert	$\rho_h = \rho \frac{\cos\theta_n}{(\cos i \cdot \cos\theta_n)^k}$	Smith et al. (1980)
Minnaert+SCS	$\rho_h = \rho \frac{(\cos\theta_s)^{k'} \cos\theta_n}{(\cos i)^{k'}}$	Reeder (2002)

where ρ_h is the surface reflectance after correction, ρ is the surface reflectance before correction, $\rho_{\min}$ is the minimum surface reflectance of the original image, C is the empirical constant, and k and k' are the Minnaert constants in the Minnaert and Minnaert+SCS models, respectively.

$$\ln\rho_h + k\ln(\cos i \cdot \cos\theta_n) = \ln(\rho\cos\theta_n), \tag{2}$$

where ρ_h is the surface reflectance after correction and θ_n is the terrain slope estimated from the DEM. We can replace $\ln(\cos i \cdot \cos\theta_n)$, $\ln(\rho\cos\theta_n)$, and $\ln\rho_h$ into x, y, and m, respectively, and hence, Eq. (2) can be represented as follows:

$$y = kx + m. \tag{3}$$

The sample data for estimating parameters C and k can be selected to exclude rough terrain, roads, and urban areas (Baraldi et al., 2010). We decided to exclude pixels with slope angles less than 10° and larger than 60°. The parameters were then calculated from the linear regression analysis by using Eqs. (1) and (3) for each spectral band. The regression method iteratively refines the estimated parameters by using the 99% confidence level. This leads to the removal of outliers.

3.2. Performance assessment of the topographic correction models

The performance evaluation of the topographic correction models was performed by comparing the reflectance difference before and after the topographic correction in the sunlit and sun-shaded slope areas. The evaluation exploits the fact that (1) the reflectance in the two areas is quite different and (2) the reflectance difference must be reduced after topographic correction. Since the sunlit and sun-shaded slope areas have lower and higher incidence angles, respectively, the two areas can be easily distinguished from an incidence angle map. Training sets used for the performance assessment can be collected from the incidence angle map by using the following equations:

$$\begin{aligned} \rho_{sdw}: &\quad 1 < \frac{i - \bar{i}}{\sigma_i} < 2 \\ \rho_{sun}: &\quad -2 < \frac{i - \bar{i}}{\sigma_i} < -1, \end{aligned} \tag{4}$$

where ρ_{sdw} and ρ_{sun} are the reflectance values in the sun-shaded slope area and sunlit slope area, respectively. i is the incidence angle, $\bar{i}$ is the mean of the incidence angles, and σ_i is the standard deviation of the incidence angles. The training sets in both slope areas include some of the pixels used for estimating parameters C and k.

Here, we introduce the HSSIM index to evaluate the correction performance. The index can indicate the probability of identifying the same land cover areas as the same objects. The HSSIM index is calculated from (i) the dispersion of reflectance values and (ii) the structural similarity of image histograms in the sunlit and sun-shaded slope areas before and after topographic correction. The index is defined by:

$$HSSIM(x,y) = V(x,y)^{\alpha} \cdot R(x,y)^{\beta}, \tag{5}$$

where x and y represent the reflectance values in the sunlit and sun-shaded slope areas, respectively. $\alpha > 0$ and $\beta > 0$ are weighting parameters used to adjust the relative importance between $V(x, y)$ and $R(x, y)$. $V(x, y)$ is the variation ratio between the original and corrected images in the x and y data as given by:

$$V(x,y) = \frac{\sigma_x \cdot \sigma_y}{\sigma_{x_0} \cdot \sigma_{y_0}}, \tag{6}$$

where σ_{x_0} and σ_{y_0} are the standard deviations in the x and y data of an original image, respectively. σ_x and σ_y are the standard deviations in the x and y data of a corrected image, respectively. $R(x, y)$ is the histogram structural similarity ratio, which is defined as follows:

$$R(x,y) = \frac{1 - r_{H(x)H(y)}}{1 - r_{H(x_0)H(y_0)}}, \tag{7}$$

where $H(x_0)$ and $H(y_0)$ are the histogram data of x and y in the original image, respectively. $H(x)$ and $H(y)$ are the x and y histogram data in the corrected image, respectively. $r_{H(x_0)H(y_0)}$ is the correlation coefficient between the x and y histogram data in the original image, and $r_{H(x)H(y)}$ is the correlation coefficient in the corrected image. The correlation coefficient is calculated as given by (Eskicioglu and Fisher, 1995):

$$r_{H(x)H(y)} = \frac{\sum_{i=1}^{n}(H_x(i) - \overline{H_x}) \cdot (H_y(i) - \overline{H_y})}{\sqrt{\sum_{i=1}^{n}(H_x(i) - \overline{H_x})^2 \cdot \sum_{i=1}^{n}(H_y(i) - \overline{H_y})^2}}, \tag{8}$$

where $H_x(i)$ and $H_y(i)$ are the reflectance values of the i-th bin of the histograms in the x and y histogram data, respectively. $\overline{H_x}$ and $\overline{H_y}$ are the means of the x and y data, respectively.

The variation ratio $V(x, y)$ compares the standard deviation differences before and after topographic correction in the sunlit and sun-shaded slope areas. In general, the dispersion of reflectance values in the sunlit slope area is larger than that in the sun-shaded slope area. This produces a higher standard deviation in the sunlit slope area than that in the sun-shaded slope area. Supposing that the topographic correction works well, the standard deviation of the corrected image must be smaller in the sunlit slope area according to the decreased reflectance values. On the other hand, the standard deviation in the sun-shaded slope area can increase after correction. A very high standard deviation in the corrected sun-shaded slope area means that the result has been over-corrected. Thus, we can evaluate whether the data have been corrected well or not through the variation ratio. The correction is well done if the variation ratio is very close to zero; meanwhile, the topographic effect causes no variation if ($V(x, y) = 1$), and the topographic effect is over-corrected if ($V(x, y) > 1$), i.e., when the variation ratio is larger than 1.

The histogram structural similarity ratio $R(x, y)$ compares the histogram similarity between the sunlit and sun-shaded slope areas before and after topographic correction. The $R(x, y)$ is calculated by using the correlation coefficient between the two image histograms extracted from the sunlit and sun-shaded slope areas. The ideal value for $R(x, y)$ is zero, which is obtained when the histogram correlation coefficient after topographic correction is 1. The $R(x, y)$ works similarly to $V(x, y)$. The topographic effect causes no variation when $R(x, y) = 1$, and the topographic effect is over-corrected when $R(x, y) > 1$.

The HSSIM index will produce different values depending on the weights α and β. A value of 1 as the weight is appropriate when we do not consider the relative importance of the two factors. The variation ratio can be emphasized as more important by setting the α weight to be relatively larger than the β weight when calculating the HSSIM index. On the other hand, the HSSIM ratio can be highlighted by having a larger β weight. If the $V(x, y)$ and $R(x, y)$ show that one is corrected and the other is over-corrected, the HSSIM value may be larger or lesser than 1 depending on the weights. If both the $V(x, y)$ and $R(x, y)$ are over-corrected ($V(x, y) > 1$ and $R(x, y) > 1$), the HSSIM index will unconditionally be larger than 1 regardless of the weights. Conversely, if the topographic effect is well corrected and both $V(x, y)$ and $R(x, y)$ are less than 1, the index will also be smaller than 1 regardless of the weights. Consequently, the HSSIM index indicates that (i) the topographic correction is perfectly done if it is close to 0 and (ii) the topographic correction is not properly applied if it is larger than 1.

This HSSIM index can be used for comparing the performance among topographic correction methods. Various topographic correction methods have been proposed (see Table 2), and the best topographic correction method can be different according to the spectral band used and surface type. Therefore, the HSSIM index can be effectively used to select the best topographic correction method.

4. Results and discussion

4.1. Topographic correction

Fig. 2 shows the results of the regression analysis for estimating parameter C (Fig. 2a) and k (Fig. 2b) in the SWIR-1 band of test image 1. In Fig. 2a, the offset and slope estimated by the linear regression analysis were about 0.074 and 0.010, respectively. Consequently, the empirical parameter C was about 7.4 with a low RMSE of 0.004. To estimate the Minnaert parameter k, the slope was calculated as shown in Fig. 2b. The estimated constant k was about 0.277 with a RMSE of 0.031. The parameters C and k were estimated for each spectral band though the above procedure.

Figs. 3–5 show the true color composite Landsat-8 OLI red, green, and blue bands, respectively, to highlight the difference between the results. These results are located in the visible analysis area of Fig. 1d. The results showed that several topographic correction methods well compensated for the topographic effects in the sun-shaded area and sunlit area. In the deciduous forest (Fig. 3), following application of the statistical-empirical, C-correction, and SCS+C models, the topographic effects seemed to be removed properly (Fig. 3c, d, and f). However, the cosine and SCS models produced severely over-corrected results (Fig. 3b and e). Furthermore, the reflectance values of shadowed and sunlit slopes were reversed. The C-HuangWei, Minnaert, and Minnaert+SCS models also did not lead to proper corrections in the RGB composite images, as seen in Fig. 3g, h, and i. The results of the C-HuangWei model showed that the shadow effects still remained in the sun-shaded slopes. The images from the Minnaert and Minnaert+SCS models tended to be over-corrected because the blue colors were deeper than those in the original image. Fig. 4 shows the correction results from the broad-leaved deciduous forest. A fine performance was achieved in terms of eliminating the topographic effect by the statistical-empirical, C-correction, and SCS+C models. The Minnaert and Minnaert+SCS models did not correct the data as well as the models described above. While the topographic effect was compensated compared with the original images, the outlines of the mountains still remained in the corrected images. On the other hand, the results of the cosine and SCS methods showed over-corrections like in Fig. 3. This means that they displayed the same performance in the same land cover types. These results in vegetated areas were similar to those of other researchers. Specifically, irrigated land and steppe cultivated areas (Vicente-Serrano et al., 2008), agricultural regions (Moreira and Valeriano, 2014), and shrub areas (Gao et al., 2014) all showed good correction results with non-Lambertian correction techniques. Thus, our results support such a tendency.

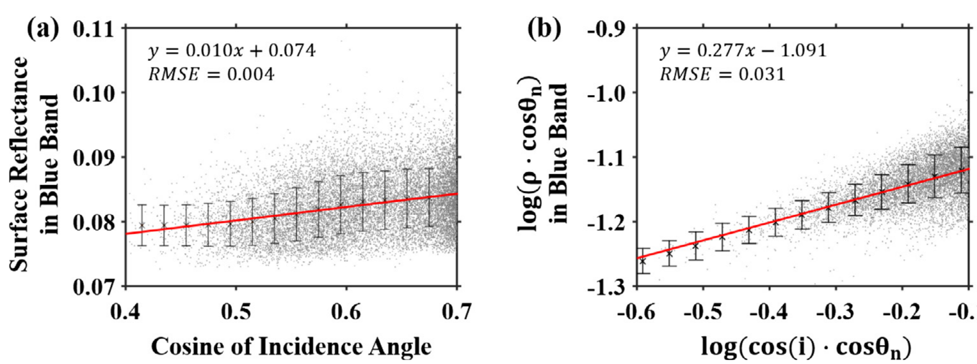

Fig. 2. Estimations of the parameters (a) C and (b) k for the SWIR-1 band in the deciduous forest sample derived by the regression analysis.

Please cite this article in press as: Park, S.-H., et al. A quantitative method to evaluate the performance of topographic correction models used to improve land cover identification. Adv. Space Res. (2017), http://dx.doi.org/10.1016/j.asr.2017.06.054

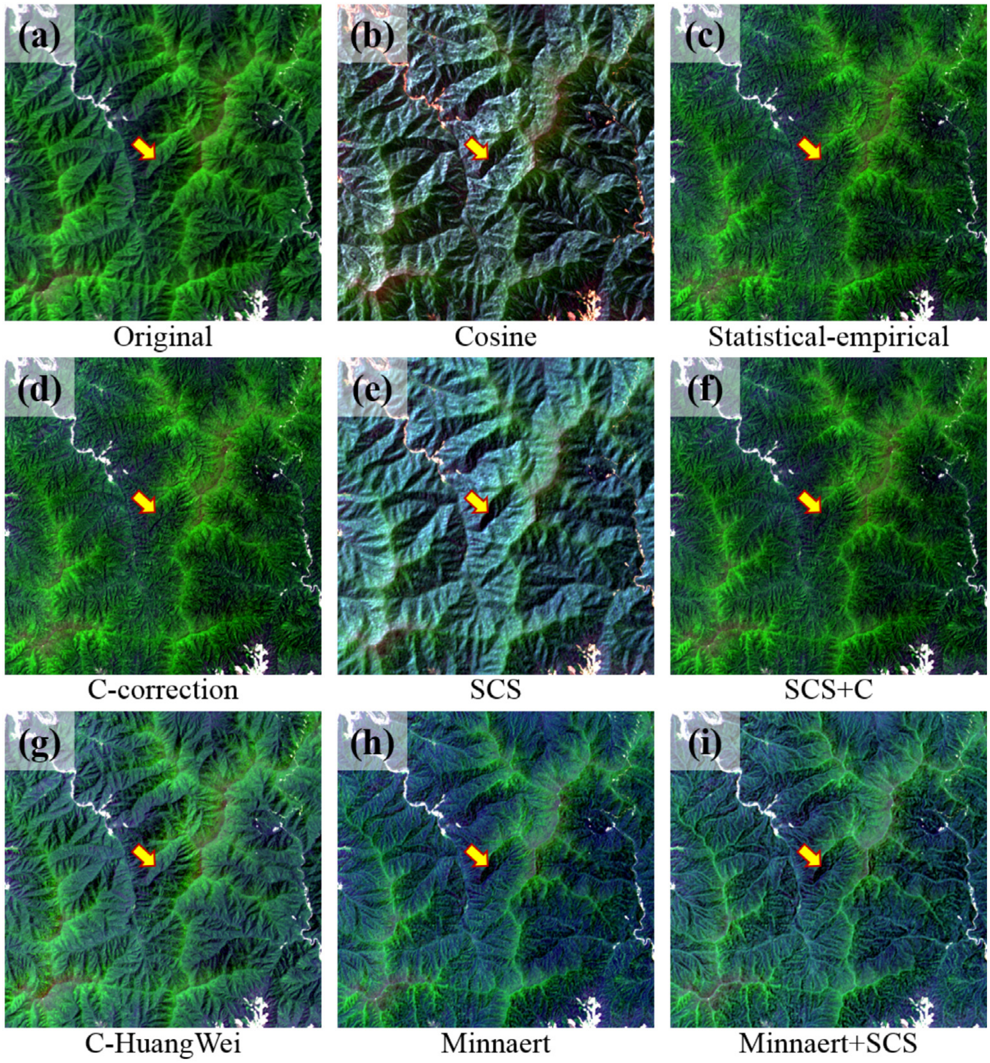

Fig. 3. Topography-corrected images in the deciduous forest area: (a) original image; (b) cosine model; (c) statistical-empirical model; (d) C-correction model; (e) SCS model; (f) SCS+C model; (g) C-HuangWei model; (h) Minnaert model; (i) Minnaert+SCS model. All images show Landsat OLI bands 4, 3, and 2 as red, green, and blue, respectively. (For interpretation of the references to color in this figure legend, the reader is referred to the web version of this article.)

Notably, the results can change when external factors such as snow or rain affect the land cover (Fig. 5). Typically, snowfall will cause different image identification results by changing the reflectance of the surface. In addition, snowfall melts rapidly on sunlit slopes but slowly on sun-shaded slopes. Thus, sun-shaded slopes maintain the reflectivity characteristics of snow for a long time, but sunlit slopes have mixed characteristics in terms of the original reflectance of the surface and the reflectance of snow because portions of the snow melt and disappear (Dedieu et al., 2016; Kour et al., 2016). In this study, the cosine, SCS, and C-HuangWei corrections models tried to compensate for the topographic effects, but the data were not corrected perfectly. The statistical-empirical, C-correction, SCS+C, Minnaert, and Minnaert+SCS methods resulted in little change or no change after correction, which was mainly due to the difficulty in estimating the relationship between the reflectance and incidence angles. This result was similar to the study conducted by Singh et al. (2015). They carried out topographical corrections with five AWiFS (Advanced Wide Field Sensor) and MODIS (Moderate Resolution Imaging Spectroradiometer) images of the snow-covered Himalayan region and reported that the cosine, C-correction, Minnaert, and SCS+C models were not very successful and produced poor results.

4.2. Performance assessment of the topographic corrections

To evaluate the performance of the topographic correction models quantitatively, we estimated the HSSIM index between the sunlit and sun-shaded slopes within the whole study area. Fig. 6 shows the collected training sets within the visible analysis area obtained by using Eq. (4). The training sets were mostly located along the mountain slopes because the surface reflectance values were different on both sides in this region.

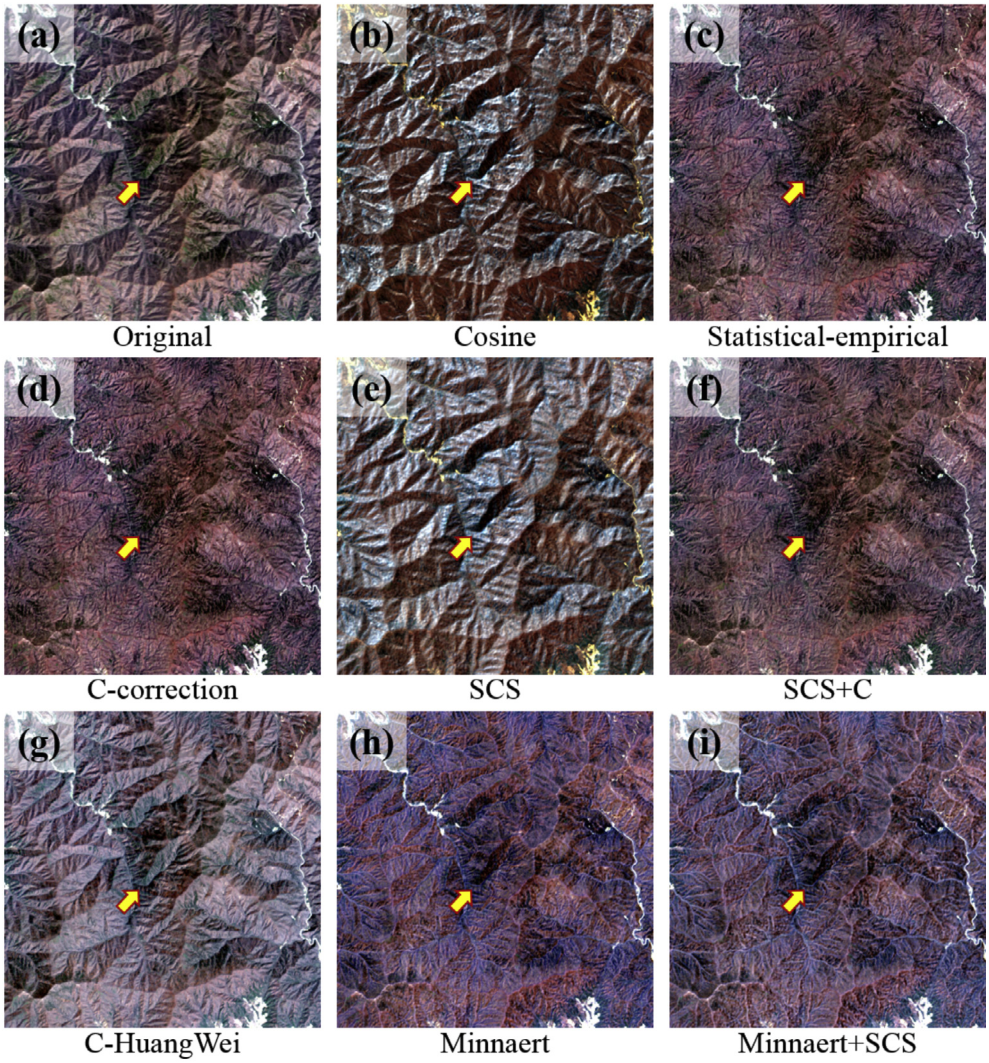

Fig. 4. Topography-corrected images in broad-leaved deciduous forest: (a) original image; (b) cosine model; (c) statistical-empirical model; (d) C-correction model; (e) SCS model; (f) SCS+C model; (g) C-HuangWei model; (h) Minnaert model; (i) Minnaert+SCS model. All images show Landsat OLI bands 4, 3, and 2 as red, green, and blue, respectively. (For interpretation of the references to color in this figure legend, the reader is referred to the web version of this article.)

Fig. 7 shows the image histograms calculated from the training sets in test image 1. The gray color and white color represent the sun-shaded and sunlit slopes, respectively. In the near infrared (NIR), SWIR-1, and SWIR-2 bands of the original image, the sun-shaded and sunlit areas can be easily distinguished because the sunlit area had a higher reflectance value than the sun-shaded area. There were overlapping areas in the histograms of the green and red bands, but slight differences were detected at the peak of the histograms. The difference of reflectance values in the dominant region of the histogram caused the topographic effect in the original image. Otherwise, the blue band did not seem to be needed to correct the topographic effects because there was almost no difference within the histograms.

As with the blue band in the original image, if the correction model demonstrated perfect performance, the mean difference between the two histograms should be zero, and the histograms should have a similar distribution. From the visual analysis using an RGB composite image, we observed that the statistical-empirical, C-correction, and SCS+C models showed excellent performance. They showed the highest performance because their histograms were well fitted. Application of the cosine and SCS models resulted in reversed images compared to those of the original images, and the sun-shaded area had a higher reflectance than the sunlit area in the visual bands. These results clearly showed over-corrected values in the visible analysis. In the case of the Minnaert and Minnaert+SCS models, the histograms were slightly reversed similar to the cosine and SCS correction in the RGB bands, but the mean differences were largely decreased. In the NIR band, most of the topographic correction methods tried to minimize the topographic effects, but they did not fully correct the images. Both the statistical-empirical and Minnaert +SCS models showed fine results, but there were small

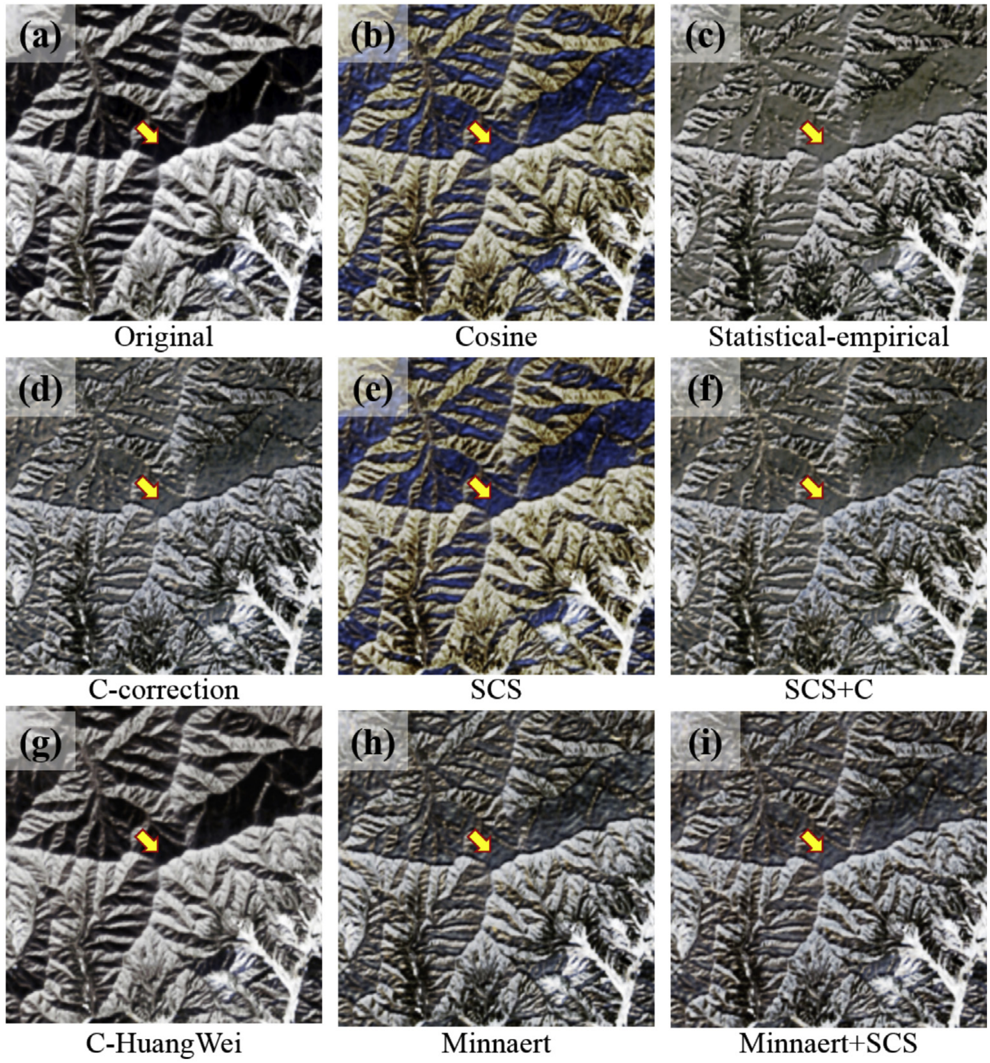

Fig. 5. Topography-corrected images in the snow-covered area: (a) original image; (b) cosine model; (c) statistical-empirical model; (d) C-correction model; (e) SCS model; (f) SCS+C model; (g) C-HuangWei model; (h) Minnaert model; (i) Minnaert+SCS model. All images show Landsat OLI bands 4, 3, and 2 as red, green, and blue, respectively. (For interpretation of the references to color in this figure legend, the reader is referred to the web version of this article.)

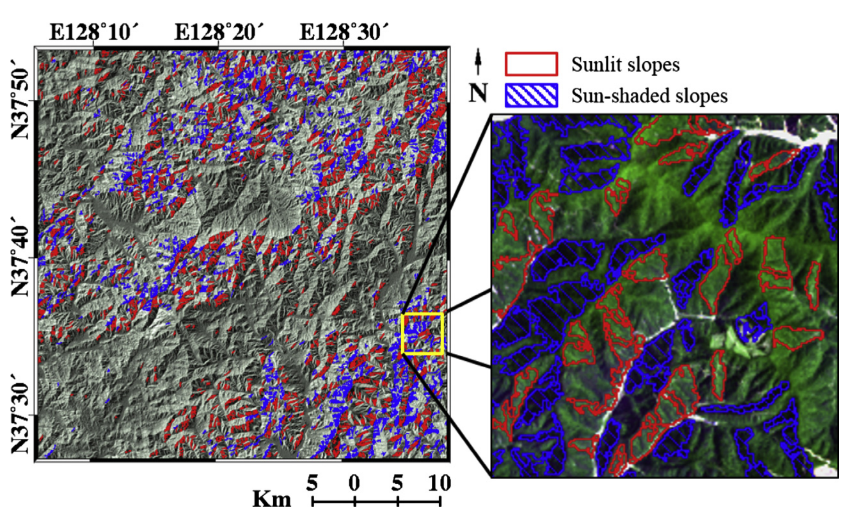

Fig. 6. Training sets used for this study. Red lines indicate the sunlit slopes and blue lines indicate the sun-shaded slopes. (For interpretation of the references to color in this figure legend, the reader is referred to the web version of this article.)

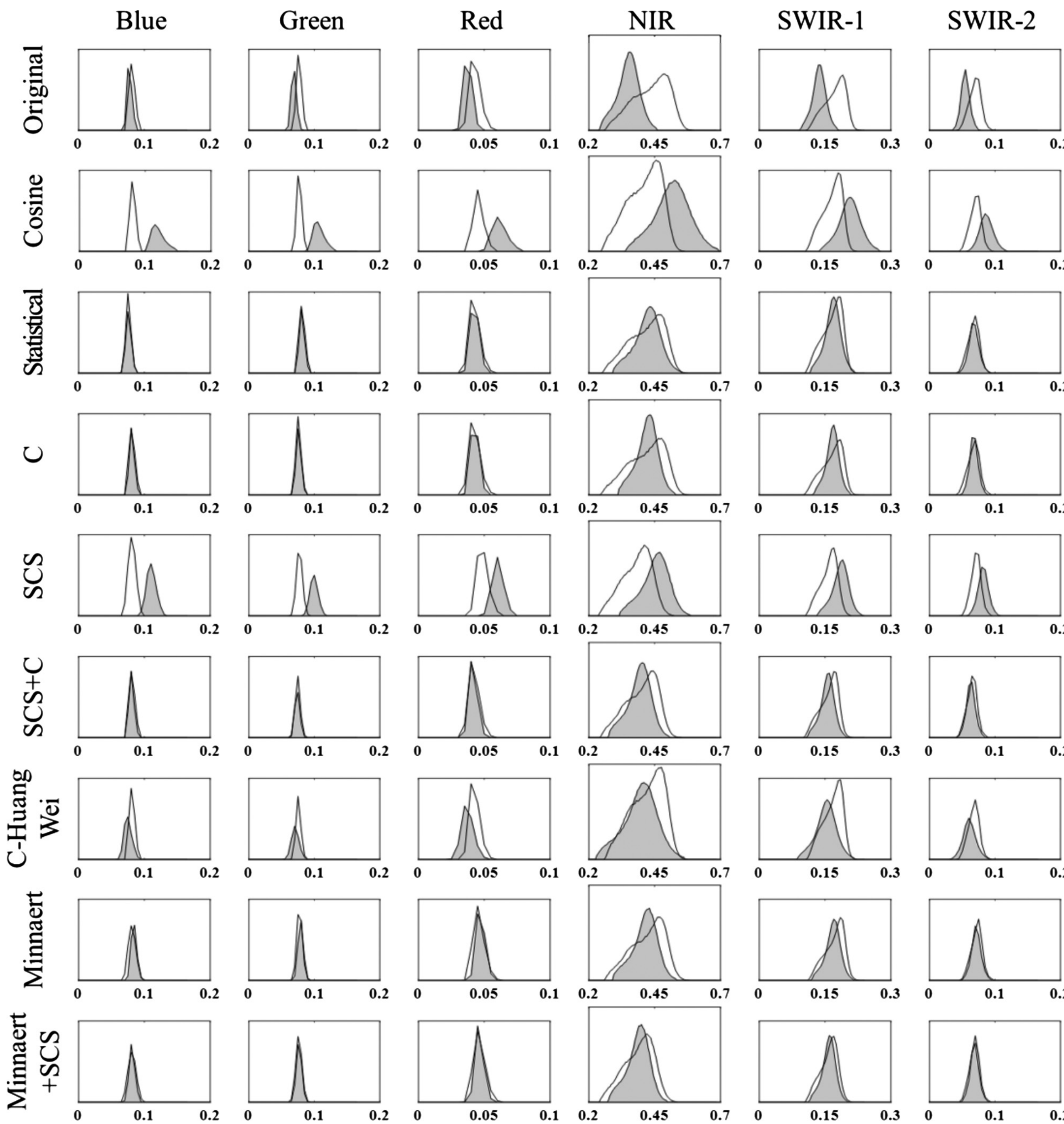

Fig. 7. Similarity between both areas before and after corrections in the deciduous forest area. The gray and white colors represent the sun-shaded slope and sunlit slope, respectively.

differences between both histograms. The statistical-empirical and Minnaert+SCS models were successful in minimizing the topographic effects of the SWIR-1 and SWIR-2 bands, respectively.

Table 3 shows an example of the HSSIM index calculation process for the NIR band in the deciduous forest area (test image 1). The standard deviations for the sunlit slope ($\boldsymbol{\sigma}_{x_0}$) and sun-shaded slope ($\boldsymbol{\sigma}_{y_0}$) in the original image were 0.07 and 0.04, respectively. The correlation coefficient ($\gamma_{H(x_0)H(y_0)}$) between the sunlit slope and sun-shaded slope in the original image was 0.23. As addressed in the methods section, the standard deviation was larger in the sunlit slope area. The ideal correction model should reduce the standard deviation in the sunlit slope area and maintain the standard deviation in the sun-shaded slope area. The SCS+C and Minnaert+SCS models performed this faithfully. On the other hand, the other models showed that changes to the two standard deviations had a trade-off relationship. The variation ratio ($V(x,y)$) was calculated by the variation of the standard deviation for both slopes. The $V(x,y)$ of the cosine and C-HuangWei models were larger than 1, which means that the topographic effect was

Table 3
Example of the histogram structural similarity (HSSIM) index calculation process for the NIR band in the deciduous forest area.

	σ_x	σ_y	$\gamma_{H(x)H(y)}$	$V(x,y)$	$R(x,y)$	HSSIM ($\alpha = 1$, $\beta = 1$)	HSSIM ($\alpha = 2$, $\beta = 1$)
Original Image (before correction)	0.07	0.04	0.23	1.00	1.00	1.00	1.00
Cosine	0.06	0.07	0.13	1.51	1.13	1.70	2.57
Statistical-empirical	0.07	0.05	0.89	1.15	0.14	0.16	0.19
C-correction	0.07	0.04	0.80	0.99	0.27	0.26	0.26
SCS	0.06	0.05	0.42	1.00	0.76	0.75	0.75
SCS+C	0.06	0.04	0.84	0.94	0.21	0.20	0.19
C-HuangWei	0.06	0.06	0.83	1.43	0.22	0.32	0.46
Minnaert	0.06	0.05	0.82	1.03	0.24	0.24	0.25
Minnaert+SCS	0.06	0.04	0.92	0.85	0.10	0.09	0.08

over-corrected. Other models except the Minnaert+SCS showed a value of about 1. The standard deviation in the sunlit slope area was reduced, but it was increased in the sun-shaded slope area. The performance of the Minnaert +SCS model was the best. This model reduced the standard deviation in the sunlit slope area while preserving the standard deviation in the sun-shaded slope area. The histogram structural similarity ratio ($R(x, y)$) was calculated by using Eq. (7). Only the cosine model yielded a value larger than 1, which means that this model caused over-correction. The corrected images produced by the other models showed higher correlations than the original image. They produced $R(x, y)$ values close to zero; the smallest value was found with the Minnaert+SCS model. The HSSIM index was calculated from the multiplication of $V(x, y)$ and $R(x, y)$, and different values were obtained depending on the weights. The HSSIM index of the cosine, statistical-empirical, C-HuangWei, and Minnaert models increased when $V(x, y)$ was emphasized. These $V(x, y)$ values were larger than 1. The Minnaert+SCS model, which showed good performance at both ratios, was selected as the best model because the calculations produced the closest values to zero.

Table 4 summarizes the HSSIM index values for the topographic corrections of test image 1. We did not consider the weights because there was no problem in selecting the best model. It is important to note that the HSSIM index represents the normalization of the reflectance in the sunlit and sun-shaded slope areas. We can see that the two Lambertian approaches (the cosine and SCS) were limited in the correction of the topographic effect when compared to the other models. The HSSIM indices were much larger than 1. In addition, it can be observed that the statistical-empirical, C-correction, and SCS+C models displayed better performance in the R, G, B, and SWIR-2 bands compared to the NIR and SWIR-1 bands. The C-HuangWei model tried to compensate for the topographic effect, but its performance was limited. The HSSIM index values of the C-HuangWei model in the R, G, and B bands were larger than those in the NIR, SWIR-1, and SWIR-2 bands. This means that the C-HuangWei model over-corrected the topographic effect in the R, G, and B bands. The Minnaert and Minnaert+SCS corrections did work well in all bands except the B band. Rayleigh scattering is more effective at short wavelengths. Thus, the reflectance values of both slopes were already similar in the original B band. The following results show how the topographic correction was evaluated by using the proposed HSSIM index values. For the blue band region, the best HSSIM index values were obtained by the statistical-empirical model (0.07), followed by the SCS+C (0.10) and C-correction (0.11) models. In the case of the green band region, the HSSIM index values obtained by the statistical-empirical model were the best (0.00), followed by those of the C-correction (0.00) and Minnaert+SCS (0.01) models. The topographic correction of the green band was better than that of the blue. For the red band region, the HSSIM index values obtained by the statistical-empirical model were the best (0.02), followed by those of the SCS+C (0.03) and C-correction (0.04) models. In the NIR band region, unlike the R, G, and B bands, the HSSIM index values obtained by the Minnaert+SCS

Table 4
Similarity between both areas before and after corrections using the HSSIM in the deciduous forest area. The best performance models are highlighted in bold.

HSSIM	Blue band	Green band	Red band	NIR band	SWIR-1 band	SWIR-2 band
Cosine	16.53	3.73	4.56	1.70	1.43	1.40
Statistical-empirical	**0.07**	**0.00**	**0.02**	0.16	0.11	0.03
C-correction	0.11	0.00	0.04	0.26	0.19	0.07
SCS	16.08	3.00	3.27	0.75	0.67	0.70
SCS+C	0.10	0.02	0.03	0.20	0.17	0.07
C-HuangWei	3.02	0.63	1.31	0.32	0.46	0.40
Minnaert	0.90	0.09	0.16	0.24	0.19	0.05
Minnaert+SCS	0.32	0.01	0.08	**0.09**	**0.06**	**0.01**

model were the best (0.09), the statistical-empirical model ranked second (0.16), and the SCS+C model ranked third (0.20). For the SWIR-1 band, the HSSIM index values calculated by the Minnaert+SCS model were the best (0.06), followed by those of the statistical-empirical (0.11) and SCS+C (0.17) models. In the SWIR-2 band region, the best model was the Minnaert+SCS (0.01), followed by the statistical-empirical (0.03) and Minnaert (0.05) models. In summary, when the performance evaluation was performed with test image 1 using the HSSIM index, the C-correction, statistical-empirical, and SCS+C models reduced the topographic effects from the blue band to the SWIR-2 band, while the cosine and SCS models did not normalize the reflectance values by the topographic effects. The C-HuangWei method worked properly in the NIR, SWIR-1, and SWIR-2 bands, but over-corrections were detected in the R, G, and B bands. The Minnaert and Minnaert+SCS models demonstrated good correction performance in the G, R, NIR, SWIR-1, and SWIR-2 bands, while the topographic effects in the B band were not well corrected. The same analysis was performed for test image 2 (Fig. 4) and test image 3 (Fig. 5). Table 5 shows a summary of all the evaluation results for all tests. In the forest cover case, the statistical-empirical model showed good performances in the R, G and B bands, while the Minnaert+SCS model showed fine results in the NIR, SWIR-1, and SWIR-2 bands. In the snow cover case, the SCS+C model was superior to the other models for the B to NIR bands, while the Minnaert+SCS method was best among the correction models. Fig. 8 shows the HSSIM indices of the topographic correction models used for these tests. As shown in Fig. 8a and b, the cosine, SCS, and C-HuangWei methods had HSSIM indices larger than 1 in the forest cover types. This means that the cosine, SCS, and C-HuangWei methods over-corrected the topographic effects in the forest cover types. In the snow cover type, all of the models except the Minnaert model corrected the data properly (see Fig. 8c). The Minnaert+SCS model was best in this case. The Minnaert model showed a good result in the visual analysis (Fig. 5), but it did not yield a fine result in terms of the HSSIM index. This is because the k parameter was larger than 1. If k is larger than 1, the average and standard deviation of the corrected image is higher than those of the original image, and hence, the HSSIM index is larger than 1.

We found overall agreement through comparing the evaluation results of this study with those of previous studies. The cosine and SCS models were found to be inappropriate in the literature (Gao and Zhang, 2009; Gao et al., 2014). These models frequently produced over-corrected results because they assume that the real surface is a Lambertian surface. In general, the other studies concluded that the C-correction, SCS+C, Minnaert, and Minnaert+SCS models could give adequate results, but there were differences in the best correction model. Moreira and Valeriano (2014) observed only small differences between the C-correction, SCS+C, and Minnaert models. They evaluated those models based on the identification accuracy, standard deviation, and relationship between spectral data and solar illumination angle. Hanston and Chuvieco (2011) found that the statistical-empirical model gave the best results when analyzing the homogeneity of different land covers after correction. They evaluated the reduction of the standard deviation for different land covers. Richter et al. (2009) reported that the C-correction model yielded better results for visible bands, but the modified Minnaert achieved better results for the NIR and SWIR bands. The performance was evaluated via the ratio between the standard deviation and mean. On the other hand, the evaluation of Gao et al. (2014) included the Minnaert+SCS model unlike other studies and they reported that the Minnaert+SCS model performed better than other models in terms of the regression fitting results.

The proposed HSSIM index can be compared with similar evaluation methods. Sola et al. (2014) proposed the SSIM method to compare the corrected image with the synthetic horizontal image. The reference image in that study was generated with ground reflection, direct, diffuse, and global horizontal irradiances. The SSIM method integrates the luminance, contrast, and structure evaluations to calculate the means SSIM (MSSIM) index as a single overall quality. The SSIM and proposed HSSIM methods are

Table 5
Performance rankings and HSSIM index values for all samples. The above models rank first, followed by the models listed below.

Samples	Blue Band	Green Band	Red Band	NIR Band	SWIR-1 Band	SWIR-2 Band
Sample No. 1	Statistical (0.07) SCS+C (0.10)	Statistical (0.00) C-correction (0.00)	Statistical (0.02) SCS+C (0.03)	Minnaert+SCS (0.09) Statistical (0.16)	Minnaert+SCS (0.06) Statistical (0.11)	Minnaert+SCS (0.01) Statistical(0.03)
Sample No. 2	Statistical (0.00) C-correction (0.01)	Statistical (0.01) C-correction (0.01)	Minnaert+SCS (0.06) Minnaert (0.08)	Minnaert (0.00) Statistical (0.00)	Minnaert+SCS (0.02) Statistical (0.03)	Minnaert+SCS (0.05) Statistical (0.06)
Sample No. 3	SCS+C (0.10) SCS (0.11)	SCS+C (0.05) Statistical (0.07)	SCS+C (0.02) Statistical (0.04)	SCS+C (0.01) Statistical (0.03)	Minnaert+SCS (0.04) C-correction (0.23)	Minnaert+SCS (0.03) C-correction (0.29)

Please cite this article in press as: Park, S.-H., et al. A quantitative method to evaluate the performance of topographic correction models used to improve land cover identification. Adv. Space Res. (2017), http://dx.doi.org/10.1016/j.asr.2017.06.054

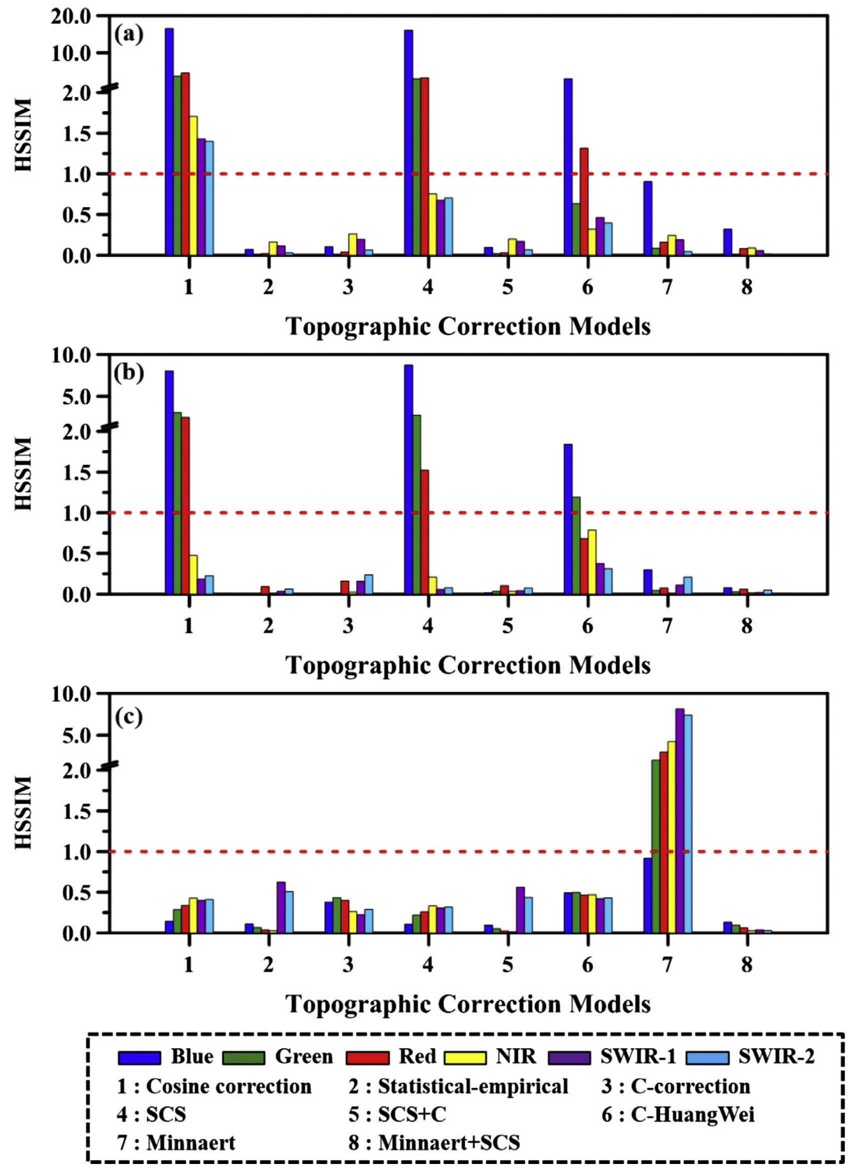

Fig. 8. Comparison of the HSSIM indices among topographic correction models in the test samples: (a) deciduous forest area; (b) broad-leaved deciduous forest; (c) snow-covered area.

advanced techniques to quantitatively evaluate topographic correction results compared to traditional methods. The traditional evaluation methods just use simple statistical parameters such as the mean, standard deviation, coefficient of determination, root mean square error, and dependence on the illumination angle for the analysis. In comparison, the SSIM and proposed HSSIM methods are more suitable for evaluating topographic correction models because these methods perform a quantitative evaluation by assuming an ideal topographically corrected result. However, there are two key differences between the proposed method and SSIM method, which are as follows. First, the SSIM evaluation method requires the synthetic horizontal image as a reference, but its procedure for producing it is complicated, yet such data are necessary to evaluate whether the synthetic image is well generated. Our proposed method shows only the similarity of two slopes after correction compared with the original image, and hence, it is simple. However, the assumption that both surfaces are of the same class should be checked. The problem of this assumption can be solved when the user selects a suitable evaluation region (the same class on different slopes) with a pre-created land surface identification map. Second, the SSIM method evaluates the best correction according to index values that are higher than the index value of the original image, but the proposed HSSIM method evaluates the correction results with numerical values based on three criteria, namely, the ideal correction ($V(x, y)$ and $R(x, y) = 0$), no variation ($V(x, y)$ and $R(x, y) = 1$), and over-correction ($V(x, y)$ or $R(x, y) > 1$). Thus, our proposed method can indentify over-corrections, and we have demonstrated this with the experimental results for the cosine and SCS models.

The proposed method does have limitations in regard to the index calculation and its application. In terms of the algorithm, it is difficult to know which index is the most effective in the evaluation because it is calculated by multiplying two ratio values. The HSSIM index value can be calculated to be close to 0 if one of the ratio values is close enough to 0 despite over-correction in the other ratio value. Also, if the variation ratio is 1, we said that this represents no variation in the methods section, but there may be a change in the standard deviation values like $V(x, y) = 0.5 * 0.8/0.8 * 0.5 = 1$. In terms of application, problems may be encountered during the collection of training sets for the topographic correction model when there is no pre-created land cover identification map. Moreover, the proposed method has not been adequately demonstrated in a study area where there are diverse land cover types.

On the basis of the results and discussion, we determined that our proposed HSSIM index could evaluate the performance of topographic correction models well at the test sites despite the above mentioned limitations. Especially, the proposed approach was found to be useful in that it can be employed to select the best method to correct for topographic effects prior to performing a land cover identification.

5. Conclusions

Several topographic correction methods have been developed to reduce topographic effects. The performance of these methods is largely dependent on the land surface types and spectral bands, and thus, it is very important to identify the best correction method according to the land surface types and spectral bands. To accomplish such a task, a quantitative method to evaluate the performance of the correction methods is required.

In this study, a quantitative method that uses the HSSIM index is proposed for evaluations of the performance of topographic correction models. The HSSIM index is estimated from the differences of the standard deviations and the histograms between the sunlit and sun-shaded slope areas before and after topographic correction. Three Landsat-8 OLI images and SRTM DEM data were used for the performance testing, and three surface cover types, which included deciduous forest, broad-leaved deciduous forest, and snow-covered areas, were evaluated. We compared the performance of several topographic correction models such as the cosine, statistical-empirical, C-correction, SCS, SCS+C, C-HuangWei, Minnaert, and Minnaert+SCS models with the proposed method. In the visual analysis, the statistical-empirical, C-correction, SCS+C, and Minnaert+SCS models performed good enough to correct the topographic effects, and all of them had low HSSIM index values in all bands. In the forest cover types, the cosine correction, SCS, and C-HuangWei models produced severely over-corrected results according to the visual analysis, and their HSSIM index values were larger than 1, which was indicative of over-correction.

We conclude with three main points that were derived from the results of this research. (i) The results confirm that the proposed HSSIM index is well-matched with the visual analysis technique except when the k parameter for the Minnaert correction is larger than 1. (ii) The best correction method can be determined in forest and snow-covered areas by using the HSSIM index values. The best correction models for the R, G, and B bands in the study site were the statistical-empirical or SCS+C models, and the best one for the NIR, SWIR-1, and SWIR-2 bands was the Minnaert+SCS model. These findings demonstrate how the proposed method enables us to evaluate the performance of topographic correction models quantitatively. (iii) It should be noted that we can combine the corrected images evaluated with the best results for each band as a hybrid image. The hybrid image should be better at estimating specific land surface types such as vegetation and snow-covered areas. Such imagery can also contribute to improved accuracy in land surface identification applications. In the future, further studies would be useful for proving that our proposed HSSIM index is valuable. These studies could include (i) direct comparisons of the proposed HSSIM method with similar evaluation methods (for example, the SIIM method) under equal criteria and (ii) studies showing that the proposed method contributes to improved land cover identification or identification accuracy in practical applications.

Acknowledgments

This work was supported by the Research and development for KMA Weather, Climate and Earth system Services (NIMS-2016-3100), funded by Earthquake and Volcano Research Division, Earthquake and Volcano Center and in part by Public Technology Development Project based on Environmental Policy (2016000210001) provided by Korea Environmental Industry and Technology Institute.

References

Baraldi, A., Gironda, M., Simonetti, D., 2010. Operational two-stage stratified topographic correction of spaceborne multispectral image employing an automatic spectral-rule-based decision-tree preliminary classifier. IEEE Trans. Geosci. Remote Sens. 48, 112–146. http://dx.doi.org/10.1109/TGRS.2009.2028017.

Blesius, L., Weirich, F., 2005. The use of the Minnaert correction for land-cover classification in mountainous terrain. Int. J. Remote Sens. 26, 3831–3851. http://dx.doi.org/10.1080/01431160500104194.

Chavez, P.S., 1996. Image-based atmospheric corrections – revisited and improved. Photogramm. Eng. Remote Sens. 62, 1025–1036.

Dedieu, J.P., Carlson, B.Z., Gigot, S., Sirguey, P., Vionnet, V., Choler, P., 2016. On the importance of high-resolution time series of optical imagery for quantifying the effects on snow cover duration on Alpine plant habit. Remote Sens. 8, 1–21. http://dx.doi.org/10.3390/rs8060481.

Dorren, L.K.A., Maier, B., Seijmonsbergen, A.C., 2003. Improved Landsat-based forest mapping in steep mountainous terrain using object-based classification. For. Ecol. Manage. 183, 31–46. http://dx.doi.org/10.1016/S0378-1127(03)00113-0.

Ediriweera, S., Pathirana, S., Danaher, T., Nichols, D., Moffiet, T., 2013. Evaluation of different topographic corrections for Landsat TM data by prediction of Foliage Projective Cover (FPC) in topographically complex landscapes. Remote Sens. 5, 6767–6789. http://dx.doi.org/10.3390/rs5126767.

Eskicioglu, A.M., Fisher, P.S., 1995. Image quality measured and their performance. IEEE Trans. Commun. 43, 2959–2965.

Gao, Y., Zhang, W., 2009. A simple empirical topographic correction method for ETM+imagery. Int. J. Remote Sens. 30, 2259–2275. http://dx.doi.org/10.1080/01431160802549336.

Gao, M.L., Zhao, W.J., Gong, Z.N., Gong, H.L., Chen, Z., Tang, X.M., 2014. Topographic correction of ZY-3 satellite images and its effects on estimation of shrub leaf biomass in mountainous areas. Remote Sens. 6, 2745–2764. http://dx.doi.org/10.3390/rs6042745.

Goslee, S.C., 2012. Topographic corrections of satellite data for regional monitoring. Photogramm. Eng. Remote Sens. 78, 973–981.

Gu, D., Gillespie, A., 1998. Topographic normalization of Landsat TM imaged of forest based on subpixel Sun-Canopy-Sensor geometry. Remote Sens. Environ. 64, 166–175. http://dx.doi.org/10.1016/S0034-4257(97)00177-6.

Gu, D., Gillespie, A.R., Adams, J.B., Weeks, R., 1999. A statistical approach for topographic correction of satellite imaged by using spatial context information. IEEE Trans. Geosci. Remote Sens. 37, 236–246. http://dx.doi.org/10.1109/36.739158.

Hanston, S., Chuvieco, E., 2011. Evaluation of different topographic correction methods for Landsat imagery. Int. J. Appl. Earth Obs. Geoinf. 13, 691–700. http://dx.doi.org/10.1016/j.jag.2011.05.001.

Huang, W., Zhang, L.P., Li, P.X., 2005. An improved topographic correction approach for satellite image. J. Image Graph. 10, 1124–1128 (in Chinese).

Irons, J.R., Dwyer, J.L., Barsi, J.A., 2012. The next Landsat satellite: the Landsat data continuity mission. Remote Sens. Environ. 122, 11–21. http://dx.doi.org/10.1016/j.rse.2011.08.026.

Kour, R., Patel, N., Krishna, A.P., 2016. Influence of shadow on the thermal and optical snow indices and their interrelationship. Remote Sens. Environ. 187, 119–129. http://dx.doi.org/10.1016/j.rse.2016.10.017.

Meyer, P., Itten, K.L., Kellenberger, T., Sandmeier, S., Sandmeier, R., 1993. Radiometric corrections of topographically induced effects on Landsat TM data in an alpine environment. ISPRS J. Photogramm. Remote Sens. 48, 17–28. http://dx.doi.org/10.1016/0924-2716(93)90028-L.

Mishra, V.D., Sharma, J.K., Singh, K.K., Thakur, N.K., Kumar, M., 2009. Assessment of different topographic corrections in AWiFS satellite imagery of Himalaya terrain. J. Earth Syst. Sci. 118, 11–26. http://dx.doi.org/10.1007/s12040-009-0002-0.

Moreira, E.P., Valeriano, M.M., 2014. Application and evaluation of topographic correction methods to improve land cover mapping using object-based classification. Int. J. Appl. Earth Obs. Geoinf. 32, 208–217. http://dx.doi.org/10.1016/j.jag.2014.04.006.

Reddy, M.B., Blah, B., 2009. Topographic normalization of satellite imagery for image classification in northeast India. Prog. Phys. Geogr. 33, 815–836. http://dx.doi.org/10.1177/0309133309351048.

Reeder, D.H., 2002. Topographic Correction of Satellite Images: Theory and Application (Ph.D. Dissertation). Dartmouth College, Hanover, New Hampshire.

Reese, H., Olsson, H., 2011. C-correction of optical satellite data over alpine vegetation areas: a comparison of sampling strategies for determining the empirical c-parameter. Remote Sens. Environ. 115, 1387–1400. http://dx.doi.org/10.1016/j.rse.2011.01.019.

Ren, G., Zhu, A.X., Wang, W., Xiao, W., Huang, Y., Li, G., et al., 2009. A hierarchical approach coupled with coarse DEM information for improving the efficiency and accuracy of forest mapping over very rugged terrains. For. Ecol. Manage. 258, 26–34. http://dx.doi.org/10.1016/j.foreco.2009.03.043.

Reuter, H.I., Nelson, A., Jarvis, A., 2007. An evaluation of void filling interpolation methods for SRTM data. Int. J. Geogr. Inf. Sci. 21, 983–1008. http://dx.doi.org/10.1080/13658810601169899.

Riano, D., Chuvieco, E., Salas, F.J., Aguado, I., 2003. Assessment of different topographic corrections in Landsat TM data for mapping vegetation types. IEEE Trans. Geosci. Remote Sens. 41, 1056–1061. http://dx.doi.org/10.1109/TGRS.2003.811693.

Richter, R., 1997. Correction of atmospheric and topographic effects for high spatial resolution satellite imagery. Int. J. Remote Sens. 18, 1099–1111. http://dx.doi.org/10.1080/014311697218593.

Richter, R., 1998. Correction of satellite imagery over mountainous terrain. Appl. Opt. 37, 4004–4015. http://dx.doi.org/10.1364/AO.37.004004.

Richter, R., Kellenberger, T., Kaufmann, H., 2009. Comparison of topographic correction methods. Remote Sens. 1, 184–196. http://dx.doi.org/10.3390/rs1030184.

Robinson, N., 1966. Solar Radiation. Elsevier, New York.

Singh, S., Talwar, R., 2013. A systematic survey on different topographic correction techniques for rugged terrain satellite imagery. Int. J. Electron. Commun. Technol. 4, 14–18.

Singh, M., Mishra, V.D., Thakur, N.K., Sharma, J.D., 2015. Expansion of empirical-statistical based topographic correction algorithm for reflectance modeling on Himalayan terrain using AWiFS and MODIS sensor. J. Indian Soc. Remote Sens. 43, 379–393. http://dx.doi.org/10.1007/s12524-014-0414-4.

Slater, J.A., Garvey, G., Johnston, C., Haase, J., Heady, B., Kroenung, G., et al., 2006. The SRTM data finishing process and products. Photogramm. Eng. Remote Sens. 72, 237–247. http://dx.doi.org/10.14358/PERS.72.3.237.

Smith, J.A., Lin, T.L., Ranson, K.J., 1980. The Lambertian assumption and Landsat data. Photogramm. Eng. Remote Sens. 46, 1183–1189.

Soenen, S.A., Peddle, D.R., Coburn, C.S., 2005. SCS+C: a modified Sun-Canopy-Sensor topographic correction in forested terrain. IEEE Trans. Geosci. Remote Sens. 43, 2148–2159. http://dx.doi.org/10.1109/TGRS.2005.852480.

Soenen, S.A., Peddle, D.R., Coburn, C.A., Hall, R.J., Hall, F.G., 2008. Improved topographic correction of forest image data using a 3-D canopy reflectance model in multiple forward mode. Int. J. Remote Sens. 29, 1007–1027. http://dx.doi.org/10.1080/01431160701311291.

Sola, I., Gonzalez-Audicana, M., Alvarez-Mozos, J., Torres, J.L., 2014. Synthetic images for evaluating topographic correction algorithms. IEEE Trans. Geosci. Remote Sens. 52, 1799–1810. http://dx.doi.org/10.1109/TGRS.2013.2255296.

Srivastava, P.K., Han, D.W., Rico-Ramirez, M.A., Bray, M., Islam, T., 2012. Selection of classification techniques for land use/land cover change investigation. Adv. Space Res. 50, 1250–1265. http://dx.doi.org/10.1016/j.asr.2012.06.032.

Su, Y., Guo, Q., 2014. A practical method for SRTM DEM correction over vegetated mountain areas. ISPRS-J. Photogramm. Remote Sens. 87, 216–228. http://dx.doi.org/10.1016/j.isprsjprs.2013.11.009.

Szuster, B.W., Chen, Q., Borger, M., 2011. A comparison of classification techniques to support land cover and land use analysis in tropical coastal zones. Appl. Geogr. 31, 525–532. http://dx.doi.org/10.1016/j.apgeog.2010.11.007.

Teillet, P.M., Guindon, B., Goodenough, D.G., 1982. On the slope-aspect correction of multispectral scanner data. Can. J. Remote Sens. 8, 84–106. http://dx.doi.org/10.1080/07038992.1982.10855028.

Tokola, T., Sarkeala, J., Van Den Linden, M., 2001. Use of topographic correction in Landsat TM-based forest interpretation in Nepal. Int. J. Remote Sens. 22, 551–563. http://dx.doi.org/10.1080/01431160050505856.

Vanonckelen, S., Lhermittem, S., Van Rompaey, A., 2013. The effect of atmospheric and topographic correction methods on land cover classification accuracy. Int. J. Appl. Earth Obs. Geoinf. 24, 9–21. http://dx.doi.org/10.1016/j.jag.2013.02.003.

Vicente-Serrano, S.M., Perez-Cabello, F., Lasanta, T., 2008. Assessment of radiometric correction techniques in analyzing vegetation variability and change using time series of Landsat images. Remote Sens. Environ. 112, 3916–3934. http://dx.doi.org/10.1016/j.rse.2008.06.011.

Vincini, M., Frazzi, E., 2003. Multitemporal evaluation of topographic normalization methods on deciduous forest TM data. IEEE Trans. Geosci. Remote Sens. 41, 2586–2590. http://dx.doi.org/10.1109/TGRS.2003.817416.

Wei, J.L., Liu, X.N., Ding, C., Liu, M.L., Jin, M., Li, D.D., 2017. Developing a thermal characteristic index for lithology identification using thermal infrared remote sensing data. Adv. Space Res. 59, 74–87. http://dx.doi.org/10.1016/j.asr.2016.09.005.

Zhang, Z.M., De Wulf, R.R., Van Coillie, F.M.B., Verbeke, L.P.C., De Clercq, E.M., Ou, X.K., 2011. Influence of different topographic correction strategies on mountain vegetation classification accuracy in the Lancang Watershed, China. J. Appl. Remote Sens. 5, 1–21. http://dx.doi.org/10.1117/1.3569124.

Zhou, Q., Liu, X., 2004. Error analysis of grid-based slope and aspect algorithms. Photogramm. Eng. Remote Sens. 70, 957–962. http://dx.doi.org/10.14358/PERS.70.8.957.